The linkage between autumn Barents-Kara sea ice and European cold winter extremes

Di Cai (di.cai@awi.de)
Alfred Wegener Institute for Polar and Marine Research

Gerrit Lohmann
Alfred Wegener Institute for Polar and Marine Research

Xianyao Chen
Frontiers Science Center for Deep Ocean Multi-spheres and Earth System and Key Laboratory of Physical Oceanography, Ocean University of China

Monica Ionita
Alfred Wegener Institute for Polar and Marine Research

Research Article

Keywords: Arctic sea ice, atmospheric circulation, blocking, cold winter extremes

Posted Date: October 17th, 2022

DOI: https://doi.org/10.21203/rs.3.rs-2142748/v1

Abstract

Despite intense efforts to understand Arctic-midlatitudes linkages, there is no agreement on whether a causal relationship exists between sea ice reduction and the frequency of occurrence of mid-latitude weather extremes (e.g., cold spells, heatwaves, droughts). By tracking month-to-month variability based on observational data, we show that a reduced sea ice over the Barents-Kara Seas in autumn is the pacemaker for the large-scale atmospheric circulation rearrangement and the variations in blocking dynamics, steering the extreme cold winters of Europe. The European winter temperature change is a direct response to a stationary Rossby wave generated by the lower troposphere diabatic heat anomaly as a result of sea ice loss over the Barents-Kara Seas in autumn, which induces a tendency for a negative phase of North Atlantic Oscillation and an increase in the atmospheric blocking frequency over Greenland and the North Atlantic. The negative phase of the North Atlantic Oscillation and enhanced blocking are closely related and complementary, each of them being associated with and jointly shaping the spatial distribution of cold anomalies over the European continent. Our work has significant implicants for a better understanding of the Arctic-midlatitude linkage and resultant extreme cold events in mid-latitudes.

1 Introduction

Observations indicate a significant warming of the Arctic region over the recent decades, accompanied by the accelerating decline of sea ice cover in all regions and for all seasons (Screen and Simmonds, 2010; Stroeve et al. 2011; Stroeve and Notz, 2018). The linear trend of the Arctic sea ice extent in September is about − 13% per decade during 1979–2017 (Serreze and Meier, 2019). These variations in the Arctic sea-ice conditions may trigger local and remote concurrent processes, influencing the regional surface energy budget (Screen and Simmonds, 2010), atmospheric and ocean circulation patterns (Francis et al. 2009; Sévellec et al. 2017), and weather systems over Northern Hemisphere continents (Cohen et al. 2014).

Despite intense efforts to understand Arctic-midlatitudes linkages, the controversy remains regarding a causal relationship between the sea ice reduction and mid-latitude weather extremes. Several studies employ numerical models to assess their connections by forcing with reduced sea ice conditions and comparing the corresponding midlatitude temperature responses to those from simulations with high sea ice, but the results do not support robust causation (Sun et al. 2016; McCusker et al. 2016). Blackport et al. (2019) conclude that mid-latitude cooling in winter is not caused by reduced sea ice but atmospheric circulation changes that precede and then simultaneously drive cold mid-latitude winters and mild Arctic conditions. In contrast, several studies based on observations (Hopsch et al. 2012; Tang et al. 2013) and model simulations (Mori et al. 2014) do find a robust connection between cold winter extremes in northern continents and the Arctic sea-ice loss, suggesting that the latter forces the former.

Thermodynamic forcing by sea ice reductions contributes to weather events by changing the large-scale atmospheric circulation and the internal shifts in atmospheric dynamics (Overland et al. 2021). More specifically, the reduction of Arctic Sea ice in autumn, particularly over the Barents and Kara Seas (BKS) (Petoukhov and Semenov, 2010), can lead to warming and instability of the overlying atmosphere. The

resulting preferential warming of the Arctic atmospheric column further causes an increase in geopotential height thickness and a decrease in the meridional temperature gradient, which may enhance upward propagating planetary waves into the stratosphere (Honda et al. 2009) and slow the polar jet stream (Francis et al. 2009).

On one hand, sufficient wave breaking in the stratosphere is conducive to disrupting and weakening the stratospheric polar vortex (SPV), potentially triggering stratospheric warming events (Cohen et al. 2014). Weeks to months later, the weakened polar vortex transfers the circulation features descend into the troposphere and surface, evident as a negative phase of the North Atlantic Oscillation (NAO) and associated continental cooling conditions (Jaiser et al. 2013; Wegmann et al. 2020), implying an essential role for tropospheric-stratospheric coupling (Sun et al. 2016). On the other hand, weakening zonal winds increase the likelihood of slower and more amplified Rossby waves, leading to more frequent blocking (Francis and Vavrus, 2012) characterized by persistent anticyclones disrupting the steady westerly flow. Due to its large spatial extent and temporal persistence, blocking may cause large-scale circulation anomalies that substantially impact weather patterns and are often associated with significant climate anomalies (Häkkinen et al. 2011; Rimbu and Lohmann 2011; Ionita et al. 2016).

However, what remains unclear is how the atmosphere responds to the reduced autumn sea ice in the BKS on the monthly time scales. The capability of climate models to simulate atmospheric circulations, the frequency and location of blocking (Masato et al. 2013), and winter temperatures (Cohen et al. 2020) is limited, inhibiting the understanding of the physical processes involved in the response of extreme cold weather to sea ice reductions through atmospheric changes. Moreover, various extreme cold winters have occurred in the mid-latitude continents during ongoing global warming and sea ice decline (Cohen et al. 2014; Kretschmer et al. 2018), affecting individuals, agriculture, and commerce directly. Here we trace the development of atmospheric flow and the blocking frequency, to present observational evidence that a reduced sea ice extent (SIE) is affecting European extreme winter weather. In brief, the aim of this study is to answer two questions: (1) Is there a link between autumn sea ice reduction and extreme cold events in Europe? If so, (2) by what physical process does it affect the temperature anomaly?

2 Data And Methods

2.1 Data

Observations of monthly SIE time series in the Barents-Kara Seas, in autumn (SON) for the period 1979–2020, were obtained from National Snow and Ice Data Center (NSIDC, Fetterer et al. 2017). To investigate the large-scale atmospheric circulation, we used the monthly sea level pressure (SLP), the 2m temperature (T2M), geopotential height and zonal and meridional winds at 500 and 100 hPa, with a grid-point resolution of 0.25°×0.25°, in winter (DJF) from 1979/1980 to 2020/2021, which are available from the fifth generation European Centre of Medium-Range Weather Forecasts atmospheric reanalysis (ERA5, Hersbach et al. 2020). Before the analysis, all variables were detrended in order to eliminate the effects of global warming and accentuate the fluctuations.

2.2 Indices for extreme climate events

In this study, extreme climate events over Europe are captured by the monthly temperature index, TN10p, as defined by the Expert Team on Climate Change Detection and Indices (ETCCDI, Peterson et al. 2001). TN10p is an index measuring the percentage of days when the daily minimum temperature is below the 10th percentile threshold calculated for each calendar day (regarding the climatological norm) using a running 5-day window. This is a measure of the percentage of cold nights in winter. The observational daily minimum temperature (TN) has been extracted from the E-OBS database v23.1e (Cornes et al. 2018) with a spatial resolution of 0.1°×0.1°.

2.3 Computation of the 2D blocking frequency

We use the two-dimensional (2D) blocking frequency index (Scherrer et al. 2006) to investigate the impacts of the SIE anomalies in the previous autumn on the temperature conditions over Europe in the following winter. The daily Z500 from the ERA5 reanalysis data (Hersbach et al. 2020) during 1979–2020 is used to calculate the blocking frequency. The 2D blocking index is based on the evaluation of blocking conditions at every grid point and goes beyond the one-dimensional blocking index (Tibaldi and Molteni, 1990). This index are obtained in terms of the following geopotential height gradients in the south (GHGS) and north (GHGN) sides of the blocking region at given three reference latitudes:

$$GHGS = \left(Z\left(\phi_0\right) - Z\left(\phi_0 - 15^\circ\right)\right)/15^\circ$$

$$GHGN = \left(Z\left(\phi_0 + 15^\circ\right) - Z\left(\phi_0\right)\right)/15^\circ$$

where ϕ_0 is the latitude of the considered grid point.

A grid point is defined as instantaneous blocking if the conditions GHGS > 0 and GHGN < (− 10 m/degrees of latitude) are simultaneously satisfied. A blocking event is detected if continuous instantaneous blocking covers at least five consecutive days. For each winter, the blocking frequency is defined as the ratio between the total number of days of blocking events and the total number of winter days. According to Scherrer et al. (2006), blockings are detected separately at each grid point within the latitude zone 35°-75°N.

2.4 Composite analysis

Composite analyses were applied to depict the typical pattern and physical mechanism responsible for connecting between the autumn sea ice extent (SIE) in the Barents-Kara Seas and the atmospheric circulation, surface air temperature, and blocking frequency. We regarded years when the value of the time series of detrended SIE in autumn was above (below) 0.8 standard deviation as high (low) SIE years. To examine the relationship between autumn sea ice and the following European weather conditions, monthly blocking frequency and TN10p anomalies in the subsequent winter-to-autumn were also performed in composite analysis.

The threshold value used for the composite analysis does not significantly alter the results. The statistical significance of the composite maps at the 5% significance level is established by Welch's *t*-test (Welch, 1947).

3 Results

The linear detrended time series of autumn SIE over the BKS for 1979–2021 (Fig. 1) exhibits substantial interannual variability. To understand the influence of atmospheric circulation responses to different autumn sea-ice states on extreme cold events in Europe, we constructed the composite maps between the linear detrended time series of autumn SIE over the BKS for the years when the values of the index were higher than 0.8 standard deviation (high) and lower than − 0.8 standard deviation (low). Statistically, the total number of high and low autumn SIE episodes considered were the same (8 cases), as derived from Fig. 1.

The wintertime atmosphere fields under different autumn sea-ice conditions over the BKS are shown in Figs. 2 and 3. In the low SIE case, the composite map of the 100 hPa geopotential height (Z100) anomaly (Fig. 2b) exhibits a wave-like pattern. Strong anomalous easterlies dominate the circulation in response to SIE decrease over the BKS for almost the whole 50°N-70°N latitudinal band, thereby reducing westerly flow. The wind differences match the associated changes of Z100 geopotential well, with a maximum anomaly of 100 gpm over the central Arctic. Additionally, the spatial characteristics of Z100 (Fig. 2b) and 500 hPa geopotential height (Z500, Fig. 2d) suggest a weakened polar vortex from the surface to the upper troposphere. The Z500 composite (Fig. 2d) presents concentrated positive values between 90°W and 60°E, with the maxima located in the Greenland Sea. The most crucial feature corresponds to the intensification of the meridional component of the mid-troposphere circulation that is perfectly visible up and downstream of the Greenland Sea during low SIE situations.

The SLP pattern (Fig. 3b) resembles the fingerprint of the negative phase of Arctic Oscillation (AO) (Thompson and Wallace, 1998), corresponding to a positive pressure anomaly in the polar region. This structure is caused by the decrease of autumn sea ice in the BKS, which leads to the increase of SST and the strengthening of the Siberian high in winter. Weak zonal winds further result in more cold Arctic air penetrating the mid-latitudes. As such, there is significant cooling over the mid and high latitudes of the Eurasian continent, as shown in Fig. 3d, and the cooling extends southward to the whole of Europe. This pattern appears to be a "warm Arctic and cold continent" pattern (Zhang et al. 2008). Strong warming over the BKS is contrasted by considerable cooling in adjacent northern Eurasia in the following winter. Although of smaller magnitude, negative SAT anomalies also cover a large part of North America.

In the high SIE case, the combination of the strengthened polar vortex (Fig. 2a) and positive AO (Fig. 3a), which favors the mid-latitude jet stream to blow strongly and consistently from west to east, causes the cold Arctic air to be locked in the polar region, coinciding with the Eurasian warming (Fig. 3c). Notably, a comparison of the wind changes and SAT reveals a good correspondence between temperature and zonal wind changes over Europe in winter, shown in Figs. 2 and 3. Anomalous south-westerlies, bringing

warm Atlantic air in high SIE situations, are contrasted by anomalous solid north-easterly flow over this region for low SIE cases. The latter is also a distinctive feature of the extreme European winter 2005–2006 event accompanied by the anomalous north-easterly and strong cooling over the European site, according to NCEP/NCAR reanalysis data (Kalnay et al. 1996).

To highlight the impact of sea ice reduction on the atmospheric climate regimes, we illustrate the composite maps of Z100 (Fig. 4) as well as Z500 (Fig. 5) and blocking frequency (Fig. 6) anomalies for the following December to May, associated with anomalously low autumn SIE over the BKS. The primary reason for using monthly averages rather than short event durations is that we are interested in persistent conditions.

A major controlling factor for classic winter cold-air outbreaks into mid-latitudes is the occurrence of SPV disruptions and displacements over the continents. This atmospheric response can be regarded as resulting from the stationary Rossby wave generated by the warming of the lower troposphere, which is caused by the decrease in autumn sea ice cover. To better illustrate the factors contributing to SPV disruptions, Fig. 4 shows the monthly evolution of the composite Z100 anomaly for the following December to May next year. The choice of such a low stratospheric level depends on this being particularly crucial for the troposphere-stratosphere coupling (Garfinkel et al. 2017).

The positive anomalies dominated the Arctic region for most of the study period, indicating a weakening of the polar vortex associated with stratospheric warming. However, the behavior of SPV in early winter (December) differs from that in mid-winter and spring. In December (Fig. 4a), the vortex may be pushed away from the pole or split. The progressively weaker states of the SPV can be clearly seen from January (Fig. 4b) to March (Fig. 4d), mainly manifested as a positive Z100 anomaly centered over Greenland/Central Arctic. Climatologically, the SPV emerges in the autumn, reaches its strongest state in January, and gradually diminishes in the spring (Zhang et al. 2022). The geopotential height, on the contrary, remains weakened after January. The positive anomalies in February (Fig. 4c) became broader than in January (Fig. 4b), centered on the Davis Strait, and the pattern remained robust in March (Fig. 4d), with even concentrating and amplifying the positive anomaly. This pattern is not perfectly symmetrical around the North Pole, but anticyclonic anomalies are displaced toward the western hemisphere. Besides, when examining the temporal evolution of their intensities, we found that Z100 anomalies were at their most robust state in March and then gradually weakened at a slow pace in the following two months. In April (Fig. 4e), it exhibits an east-west contrast over the Arctic region, when Z100 anomalies are divided, having a significant positive center over Russia and a negative center over Canada.

Figure 5 tracks the monthly response of Z500 anomaly composite to autumn sea ice reduction, which clearly illustrates the importance of the troposphere-stratosphere coupling to the surface climate (Scaife et al. 2008). The composite map of the Z500 anomalies exhibit a higher degree of zonal symmetry in the lower stratosphere (Fig. 4b-d), but wavy signatures dominate the troposphere with little zonal symmetry. The coherence of the positive and negative anomalies in the troposphere and the lower stratosphere suggests a downward influence by anomalous behavior of SPV on the tropospheric circulation from

December to January, consistent with previous findings (e.g., Polvani and Kushner 2002; Kushner and Polvani 2004). In addition, the most crucial feature of Z500 anomalies corresponds to the dramatical intensification of the meridional component of the mid-troposphere circulation, which is perfectly visible in the following months (Fig. 5). On the contrary, high SIE episodes are characterized by an intensification of the zonal circulation (Fig. 2c).

When tracking month-by-month evolutions, we readily find pronounced north-south meanders in December (Fig. 5a), with negative anomalies in the mid-latitudes except over the northern Europe, which provided a unique dynamic setting driving cold polar air to plunge southward into Europe. In January (Fig. 5b), the pattern of Z500 anomalies begin to form prototypes, and the jet stream gradually intensifies. Two intense anticyclonic circulations develop around the west and east coasts of Greenland, while a negative Z500 anomaly can be observed over the southwestern Europe. This pattern expands slightly to the northwest with even magnifying the positive anomalies and reducing the negative ones, reaching its strongest state in February (Fig. 5c). The latter diminishes and shifts towards the Atlantic, which is relevant for the heat transport of the southern European. This leads to an enforced north-south geopotential height gradient, and thus the atmospheric flow is diverted around it with an intense flow from the north, allowing cold air to penetrate southwards. In March (Fig. 5d), the anticyclonic vortex decreases over southern Greenland, being accompanied by relatively negative Z500 anomalies. The anomalies associated with the south of the jet location are very similar to the negative pattern of the NAO, and the jet stream is located further south than its climatology. Specifically, a relatively elongated negative anomaly to the south indicates an increased meridional gradient and a strong jet stream lying to the south of the anticyclonic anomaly. As shown in Fig. 5b-d, the weakened SPV is transmitted down into the troposphere during winter, causing circulation anomalies similar to the negative phase of NAO. As such, the anomalous propagation of the Rossby waves may be the precursor to forcing the NAO signals in the troposphere. In addition, when there is a block over southern Greenland (Fig. 6d) with a negative NAO regime (Fig. 5d) in March, this will force the jet stream to proceed more or less zonally across the Atlantic in April (Fig. 5e), similar to the result from Woollings et al. (2010).

Atmospheric blocking is a large-scale mid-latitude atmospheric phenomenon primarily associated with persistent anticyclonic quasi-stationary high-pressure systems, which typically extend vertically throughout the troposphere. When the high-latitude jet stream develops large and nearly-stationary meanders (e.g., Fig. 5a), the strong westerly winds of the jet stream are diverted north and south around a dramatic reversal of streamlines, and further blocking occurs. It makes weather systems move more slowly or even become stationary (Rex, 1950), which is particularly important the formation of extreme weather events. In winter, blocking can be responsible for the equatorward advection of polar air masses and the resultant anomalous cold winter temperature (Sillmann and Croci-Maspoli, 2009).

Starting in December, a center of enhanced blocking activity over Northern Russia, coupled with a center of relatively weaker blocking activity over Greenland, is observed (Fig. 6a). The blocking activity over Greenland gradually intensifies and moves down the southwest coast of Greenland, reaching its most phase in February (Fig. 6c) before vanishing over time. The center of the blocking activity over Northern

Russia remains and subsequently shifts to couple with a center of enhanced blocking activity over the southeast coast of Greenland (Fig. 6b-c), thus the more robust flow anomaly. Interestingly, there is a persistent blocking at every longitude between the Baffin Bay and Europe from January to February. In February (Fig. 6c), the positive anomalies merge and shift southward, extending more than in January, forming one broad and a continuous intensified block across Greenland and Northern Europe. The configuration of anomalous blocking frequency in March (Fig. 6d) corresponds to Greenland blocking known to be associated with the negative NAO phase (Woollings et al. 2010), which is usually related to the splitting of the jet stream into two distinct branches (Trigo et al. 2004). In April (Fig. 6e), negative anomalies occupy most of the area with no blocking over Greenland, except for the weak positive in the narrow band in North Atlantic. Then, like other variables, the atmospheric circulation system adjusts to a stable state within a short period.

The above results suggest that the local and remote atmospheric circulations have marked responses to SIE change over the BKS. The observed anomalous atmospheric circulation patterns in the troposphere and stratosphere can differ from those attributed to NAO and blocking variability.

We examine furthermore the spatial structure of extreme cold events in Europe. Figure 7 shows the composite for TN10p anomalies due to the combined effect of these atmospheric circulation variables. The insignificant change in TN10p in December (Fig. 7a) indicates that the cold air from the Arctic has not yet penetrated southwards into mid-latitudes, and the slight warming signals in central Europe may be related to the ridges transporting warm air northward. In January (Fig. 7b), pronounced cold anomalies appeared in Europe, especially over Norway and Ireland, while the positive anomalies over Turkey resulted from the southerly inflow of warm and humid air masses from the Atlantic (Fig. 5b). The widespread pattern of extreme cold remains robust in February (Fig. 7c) with even emphasized central and western Europe, while some regions in the south experienced warmer conditions. In March (Fig. 7d), the cold European anomaly persists and extends to the east, while the warm anomalies in the southern part are expanding in coverage and extend to the northwest, but a significant cooling trend can be seen over the Iberian Peninsula. Even if there is no blocking at the same time (Fig. 6d), the predominance of these cold anomalies might still be a direct response to be the persistence of blocking situation. In April (Fig. 7e), the pattern appears opposite distributions in eastern and western European, with weaker and incoherent anomalies. The cyclonic circulation around western Europe (Fig. 5f) transports warmer Atlantic air masses to the continent, essentially shaping the general norm encompassing Europe.

The robust features revealed that persistent winter cold extremes occur in the presence of atmospheric blocking. Overall, blocking influences the local weather conditions around the block, particularly the European cold extremes are associated with mid- and high-latitude blocking over the European continent as well as the North Atlantic. Europe is the dominant region because of the configuration of a strong and meridionally tilted storm track upstream of a large landmass (Kautz et al. 2022). Northerly advection anomalies mainly cause cold anomalies over most of Europe to the east of the blocking core. Over the North Atlantic, blocking is strongly correlated with the negative phase of the NAO that itself is associated with the development of cold European winters. During the negative phase of NAO, the synoptic pattern

provides diffluent flow conditions favorable for the onset and maintenance of blocking systems (Luo et al. 2015). In addition, blocking occurs over Greenland (e.g., Fig. 6d), which is associated with the negative phase of NAO and has strong downstream impacts in Europe (Rimbu and Lohmann, 2011; Davini et al. 2012; Kretschmer et al. 2018).

4 Conclusions

In this study we have analyzed the influence of autumn sea ice loss over the BKS on the severe European extreme winters by tracking the interannual variability based on observational data. Autumn sea ice reductions over the BKS are identified to be a pacemaker for the large-scale atmospheric circulation rearrangement and the variations in blocking dynamics, steering extreme cold winters over Europe. The lower troposphere diabatic heat anomaly in the BKS sector associated with reduced sea ice is the primary source of heating and cooling in the atmospheric circulation response, exciting the upward emanation of the stationary Rossby wave trains. This further disrupts the SPV and induces the sudden stratospheric warming events, thus establishing a stratospheric path. When SPV is weaker than usual, the westerly flow is relatively slow and tends to meander. Additionally, stratospheric warming events can weaken or reverse the stratospheric winds, resulting in circulation features that eventually descend into the troposphere and surface. This downward influence mechanism explains the deformation in the spatial structure of the tropospheric circulation anomalies and the southward movement of the jet stream, contributing to a tendency for a negative phase of NAO, leading the cold events to reach extremes in Europe.

In addition to changes in large-scale atmospheric circulation, thermodynamic forcing from reduced sea ice can also contribute to weather conditions through the internal shifts in atmospheric dynamics. Especially, blocking is critical to European flow changes due to its capability to interfere with the main cyclonic westerly flow, which tends to cause persistent weather conditions around the block for 1–2 months. We demonstrate that the most critical feature of the cold European anomaly corresponds to the presence and persistence of atmospheric blocking that forms and strengthens in late winter. Cold extremes in Europe are associated with a blocking system over Greenland and the North Atlantic. However, the cold anomalies are usually not located directly below the blocking center but downstream or south of it. This is why extreme cold temperatures are most pronounced over central Europe.

The results presented here indicate that not only the atmospheric circulation realignment but also variations in blocking frequency can be crucial for the frequency of occurrence of mid-latitude weather extremes. The negative phase of NAO provides diffuse flow conditions that further facilitate the onset and sustainment of blocking systems (Luo et al. 2015). Blocking and the negative phase of NAO are closely related and complementary, each associated with and jointly shaping the spatial distribution of cold anomalies over the European continent (Rimbu et al. 2014; Wegmann et al. 2020). Specifically, cold anomalies at TN10p in large parts of Europe are mainly caused by northerly flow anomalies in the eastern part of the blocking core region, while warm anomalies in southern Europe correspond to the cyclonic circulation in the North Atlantic associated with the negative phase of NAO.

Overall, the Arctic Sea ice does not merely respond passively to climate change occurring on a global scale, but instead, its changes affect weather conditions in other regions bridging spatio-temporal scales (Lohmann et al. 2020). Our results imply that the autumn anomalous low BKS sea ice is a potential precursor to predicting severe European extremes in subsequent winters. Thus, future work in this linkage will improve our understanding of the sources of predictability of midlatitude extreme events, and ultimately advance projections and predictions of the future climate.

Declarations

Ethics approval and consent to participate

Not applicable.

Consent for publication

Not applicable.

Acknowledgements

We acknowledge support by AWI through its research infrastructure in the topic “Ocean and Cryosphere under climate change” as part of the Helmholtz Program “Changing Earth - Sustaining our Future”. Support by the Helmholtz Climate Initiative REKLIM is gratefully acknowledged. We acknowledge the National Snow and Ice Data Center (NSIDC), the European Centre of Medium-Range Weather Forecasts (ECMWF), and the Expert Team on Climate Change Detection and Indices (ETCCDI) for making their data available to us.

Statements and Declarations

Funding:

This work is supported by BMBF through the project “Abrupt Climate Shifts and Extremes over Eurasia in Response to Arctic Sea Ice Change (ACE)” under Grant 01LP2004A and the National Key R&D Program of China under Grant 2019YFA0607000 and 2019YFC1509100. X.C. has received support from the Natural Science Foundation of China under Grant 41825012. D.C. is also supported by the China Scholarship Council (202106330036).

Competing Interests:

The authors declare no relevant financial or non-financial interests.

Author Contributions:

D.C. and M.I. conceived and designed the study. D.C. carried out the analyses and produced all figures under the guidance of M.I., G.L., and X.C. And all authors contributed to the rewriting and revising of the

manuscript.

Data Availability:

No datasets were generated during this study. All data used in this study are publicly available from the sources cited in “Data and Methods”.

References

1. Blackport R, Screen JA, van der Wiel K, Richard B (2019) Minimal influence of reduced Arctic sea ice on coincident cold winters in mid-latitudes. Nat Clim Change 9:697–704. https://doi.org/10.1038/s41558-019-0551-4
2. Cohen J, Screen JA, Furtado JC et al (2014) Recent Arctic amplifica- tion and extreme mid-latitude weather. Nat Geosci 7:627–637. https://doi.org/10.1038/ngeo2234
3. Cohen J, Zhang X, Francis J et al (2020) Divergent consensuses on Arctic amplification influence on midlatitude severe winter weather. Nat Clim Chang 10:20–29. https://doi.org/10.1038/s41558-019-0662-y
4. Cornes RC, van der Schrier G, van den Besselaar EJM, Jones PD (2018) An ensemble version of the E-OBS temperature and precipitation data sets. J Geophys Res Atmos 123(17):9391–9409. https://doi.org/10.1029/2017JD028200
5. Davini P, Cagnazzo C, Gualdi S, Navarra A (2012) Bidimensional diagnostics, variability, and trends of Northern Hemisphere blocking. J Clim 25(19):6496–6509
6. Fetterer F, Knowles K, Meier W, Savoie M, Windnagel AK (2017) Updated daily. Sea ice index, version 3. [indicate subset used]. Boulder, Colorado USA. NSIDC: National Snow and Ice Data Center. https://doi.org/10.7265/N5K072F8
7. Francis J, Chen W, Leathers D, Miller J, Veron D (2009) Winter northern hemisphere weather patterns remember summer Arctic sea-ice extent. Geophys Res Lett 36:L07503. doi:10.1029/2009GL037274
8. Francis JA, Vavrus SJ (2012) Evidence linking Arctic amplification to extreme weather in mid-latitudes. Geophys Res Lett 39:L06801. https://doi.org/10.1029/2012gl051000
9. Garfinkel CI, Son SW, Song K, Aquila V, Oman LD (2017) Stratospheric variability contributed to and sustained the recent hiatus in Eurasian winter warming. Geophys Res Lett 44(1):374–382. https://doi.org/10.1002/2016GL072035
10. Häkkinen S, Rhines PB, Worthen DL (2011) Atmospheric blocking and Atlantic Multidecadal ocean variability. Science 334(6056):655–659. https://science.sciencemag.org/content/sci/334/6056/655.full.pdf
11. Hersbach H, Bell B, Berrisford P et al (2020) The ERA5 global reanalysis. Q J Roy Met Soc 146:1999–2049. https://doi.org/10.1002/qj.3803
12. Honda M, Inoue J, Yamane S (2009) Influence of low Arctic sea-ice minima on anomalously cold Eurasian winters. Geophys Res Lett 36:L08707. https://doi.org/10.1029/2008GL037079

13. Hopsch S, Cohen J, Dethloff K (2012) Analysis of a link between fall Arctic sea ice concentration and atmospheric patterns in the following winter. https://doi.org/10.3402/tellusa.v64i0.18624. Tellus 64A:18624
14. Ionita M, Scholz P, Lohmann G, Dima M, Prange M (2016) Linkages between atmospheric blocking sea ice export through Fram Strait and the Atlantic Meridional Overturning Circulation. Sci Rep 6:32881. https://doi.org/10.1038/srep32881
15. Jaiser R, Dethloff K, Handorf D, Rinke A, Cohen J (2012) Impact of sea-ice cover changes on the northern hemisphere atmospheric winter circulation. Tellus 64A:11595. doi:10.3402/tellusa.v64i0.11595
16. Kalnay E, Kanamitsu M, Kistler R, Colins W, Deaven D, Gandin L, Iredell M, Saha S, White G, Wollen J, Zhu Y, Leetmaa A, Reynolds R, Chelliah M, Ebisuzaki W, Higgins W, Janowiak J, Mo KC, Ropelewski C, Wang J, Jenne R, Joseph D (1996) The NCEP/NCAR 40-years reanalyses project. Bull Am Meteorol Soc 77:437–471
17. Kautz LA, Martius O, Pfahl S, Pinto JG, Ramos AM, Sousa PM, Woollings T (2022) Atmospheric blocking and weather extremes over the Euro-Atlantic sector – a review. Weather Clim Dynam 3:305–336. https://doi.org/10.5194/wcd-3-305-2022
18. Kretschmer M, Coumou D, Agel L, Barlow M, Tziperman E, Cohen J (2018) More-persistent weak stratospheric polar vortex states linked to cold extremes. Bull Am Meteorol Soc 99:49–60
19. Kushner PJ, Polvani LM (2006) Stratosphere–troposphere coupling in a relatively simple AGCM: impact of the seasonal cycle. J Clim 19(21):5721–5727. doi:10.1175/JCLI4007.1
20. Lohmann G, Butzin M, Eissner N, Shi X, Stepanek C (2020) Abrupt climate and weather changes across timescales. Paleoceanography and Paleoclimatology 35(9). https://doi.org/10.1029/2019PA003782. e2019PA003782
21. Luo DH, Yao Y, Dai AG, Feldstein SB (2015) The Positive North Atlantic Oscillation with Downstream Blocking and Middle East Snowstorms: The Large-Scale Environment. J Clim 28:6398–6418. https://doi.org/10.1175/Jcli-D-15-0184.1
22. Masato G, Hoskins BJ, Woollings T (2013) Winter and summer Northern Hemisphere blocking in CMIP5 models. J Clim 26(18):7044–7059
23. McCusker KE, Fyfe JC, Sigmond M (2016) Twenty-five winters of unexpected Eurasian cooling unlikely due to Arctic sea-ice loss. Nat Geosci 9:838–842
24. Mori M, Watanabe M, Shiogama H, Inoue J, Kimoto M (2014) Robust Arctic sea-ice influence on the frequent Eurasian cold winters in past decades. Nat Geosci 7:869–873. https://doi.org/10.1038/ngeo2277
25. Overland JE, Ballinger TJ, Cohen J et al (2021) How do intermittency and simultaneous processes obfuscate the Arctic influence on midlatitude winter extreme weather events? Environ Res Lett 16:043002. https://doi.org/10.1088/1748-9326/abdb5d
26. Peterson TC, Folland C, Gruza G et al (2001) Report on the Activities of the Working Group on Climate Change Detection and Related Rapporteurs 1998–2001. Geneve, Switzerland, p 143. WMO, Rep.

WCDMP-47, WMO-TD 1071

27. Petoukhov V, Semenov VA (2010) A link between reduced Barents- Kara sea ice and cold winter extremes over northern continents. J Geophys Res 115:D21111. https://doi.org/10.1029/2009jd013568
28. Polvani LM, Kushner PJ (2002) Tropospheric response to stratospheric perturbations in a relatively simple general circulation model. Geophys Res Lett 29. https://doi.org/10.1029/2001GL014284
29. Rex DF (1950) Blocking action in the middle troposphere and its effect upon regional climate. Part I. An aerological study of blocking action. Tellus 2:196–211
30. Rimbu N, Lohmann G (2011) Winter and summer blocking variability in the North Atlantic region. Evidence from long-term observational and proxy data from southwestern Greenland. Clim Past 7:543–555. doi:10.5194/cp-7-543-2011
31. Rimbu N, Lohmann G, Ionita M (2014) Interannual to multidecadal Euro-Atlantic blocking variability during winter and its relationship with extreme low temperatures in Europe. J Geophys Res 119:13621–13636. https://doi.org/10.1002/2014JD021983
32. Scaife AA, Folland CK, Alexander LV, Moberg A, Knight JR (2008) European climate extremes and the North Atlantic Oscillation. J Clim. https://doi.org/10.1175/2007JCLI1631.1
33. Scherrer SC, Croci-Maspoli M, Schwierz C, Appenzeller C (2006) Two-dimensional indices of atmospheric blocking and their statistical relationship with winter climate patterns in the Euro-Atlantic region. Int J Climatol 26(2):233–249. https://rmets.onlinelibrary.wiley.com/doi/abs/10.1002/joc.1250
34. Screen JA, Simmonds I (2010) The central role of diminishing sea ice in recent Arctic temperature amplification. Nature 464:1334–1337. https://doi.org/10.1038/nature09051
35. Serreze MC, Meier WN (2019) The Arctic's sea ice cover: Trends, variability, predictability, and comparisons to the Antarctic. Ann N Y Acad Sci 1436:36–53. https://doi.org/10.1111/nyas.13856
36. Sévellec F, Fedorov AV, Liu W (2017) Arctic sea-ice decline weakens the Atlantic meridional overturning circulation. Nat Clim Change 7:604–610. https://doi.org/10.1038/nclimate3353
37. Sillmann J, Croci-Maspoli M (2009) Present and future atmospheric blocking and its impact on European mean and extreme climate. Geophys Res Lett 36:L10702. https://doi.org/10.1029/2009GL038259
38. Stroeve J, Notz D (2018) Changing state of Arctic sea ice across all seasons. Environ Res Lett 13:103001. https://doi.org/10.1088/1748-9326/aade56
39. Stroeve J, Serreze M, Holland M, Kay J, Maslanik J, Barrett A (2011) The Arctic's rapidly shrinking sea-ice cover: a research synthesis. Clim Chang 110:1005–1027
40. Sun L, Perlwitz J, Hoerling M (2016) What caused the recent "warm Arctic, cold continents" trend pattern in winter temperatures? Geophys Res Lett 43:5345–5352
41. Tang Q, Zhang X, Yang X, Francis JA (2013) Cold winter extremes in northern continents linked to Arctic sea ice loss. Environ Res Lett 8:14036. https://doi.org/10.1088/1748-9326/8/1/014036

42. Thompson DWJ, Wallace JM (1998) The Arctic oscillation signature in the wintertime geopotential height and temperature fields. Geophys Res Lett 25(9):1297–1300. https://doi.org/10.1029/98GL00950
43. Tibaldi S, Molteni F (1990) On the operational predict- ability of blocking. Tellus A 42:343–365. https://doi.org/10.1034/j.1600-0870.1990.t01-2-00003.x
44. Trigo RM, Trigo IF, DaCamara CC, Osborn TJ (2004) Climate impact of the European winter blocking episodes from the NCEP/NCAR Reanalyses. Clim Dyn 23:17–28
45. Wegmann M, Rohrer M, Santolaria-Otín M, Lohmann G (2020) Eurasian autumn snow link to winter North Atlantic Oscillation is strongest for Arctic warming periods. Earth Syst Dynam 11:509–524. https://doi.org/10.5194/esd-11-509-2020
46. Welch B (1947) The generalization of “student’s” problem when several different population variances are involved. Biometrika 34(1–2):28–35. https://doi.org/10.1093/biomet/34.1-2.28
47. Woollings T, Hannachi A, Hoskins B, Turner A (2010) A regime view of the North Atlantic Oscillation and its response to anthropogenic forcing. J Clim 23:1291–1307
48. Zhang X, Fu YF, Han Z et al (2022) Extreme cold events from East Asia to North America in winter 2020/21: Comparisons, causes, and future implications. Adv Atmos Sci 39(4):553–565. https://doi.org/10.1007/s00376-021-1229-1
49. Zhang X, Sorteberg A, Zhang J, Gerdes R, Comiso JC (2008) Recent radical shifts of atmospheric circulations and rapid changes in Arctic climate system. Geophys Res Lett 35:L22701

Figures

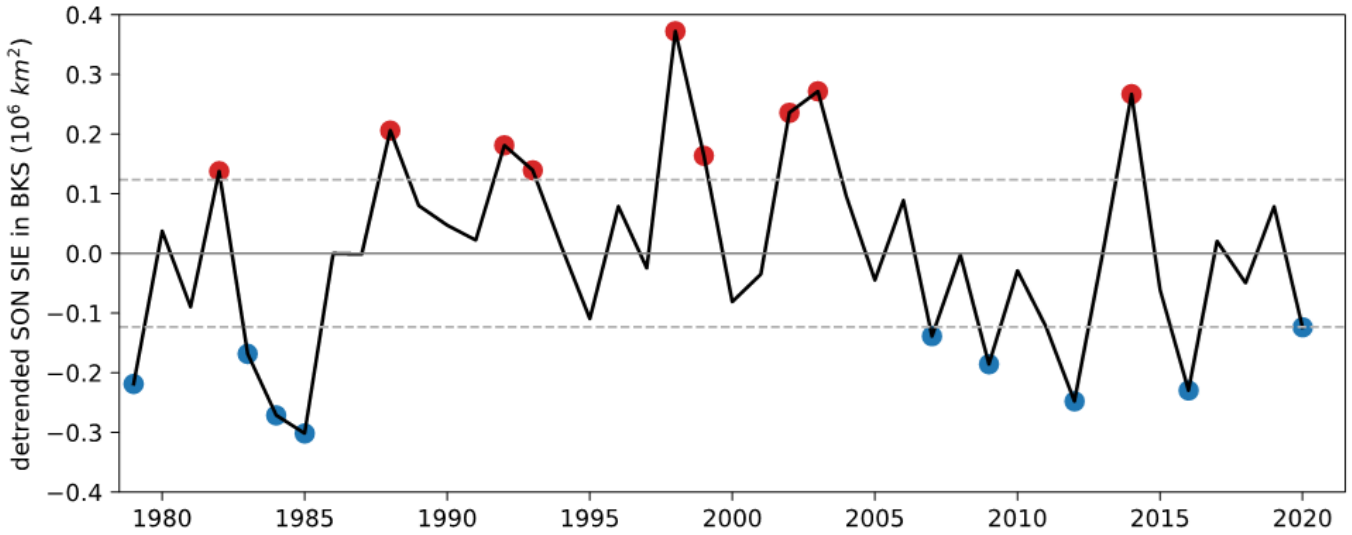

Figure 1

The linear detrended autumn SIE over the BKS from 1979 to 2021 in NSIDC observations (Fetterer et al. 2017). Years when the SIE was above and below 0.8 standard deviationare indicated by red and blue dots, respectively

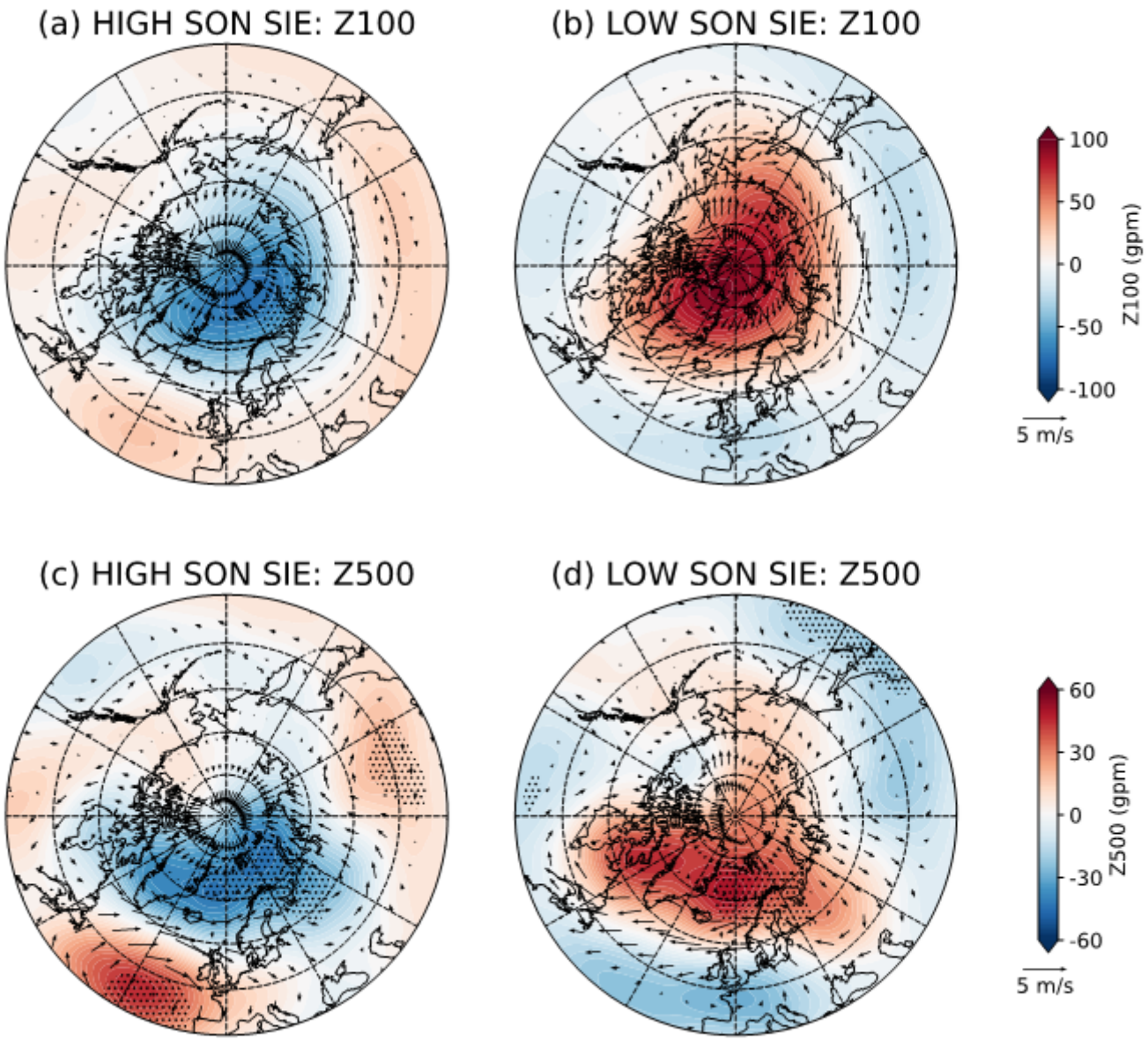

Figure 2

Composite maps for the Z100 (a, b) and Z500 (c, d) for winter (DJF) relative to the detrended autumn SIE in BKS above (left) and below (right) 0.8 standard deviation. The dots highlight significant anomalies at a confidence level of 95%

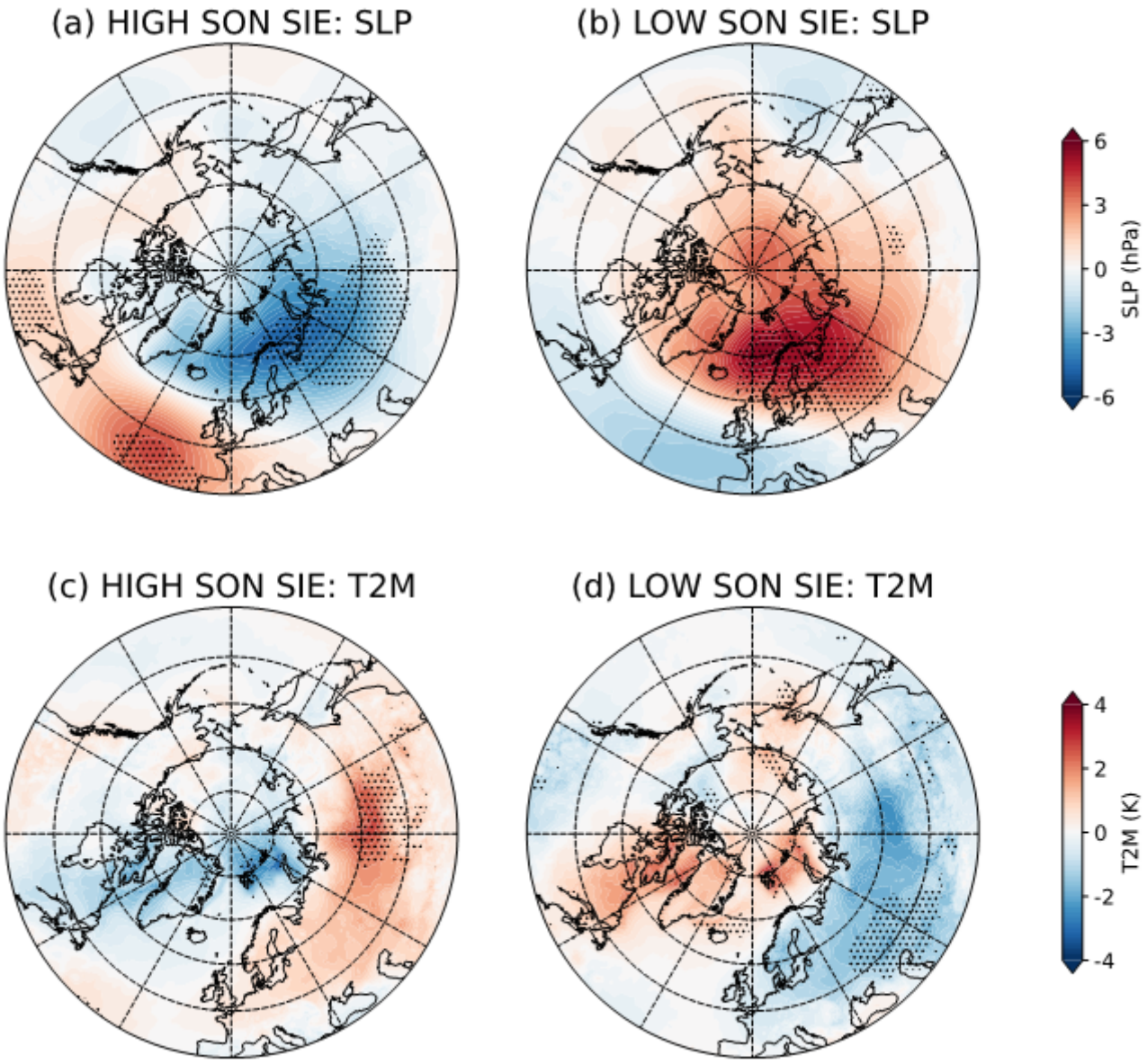

Figure 3

Composite maps for the SLP (a, b) and T2M (c, d) for winter (DJF) relative to the detrended autumn SIE in BKS above (left) and below (right) 0.8 standard deviation. The dots highlight significant anomalies at a confidence level of 95%

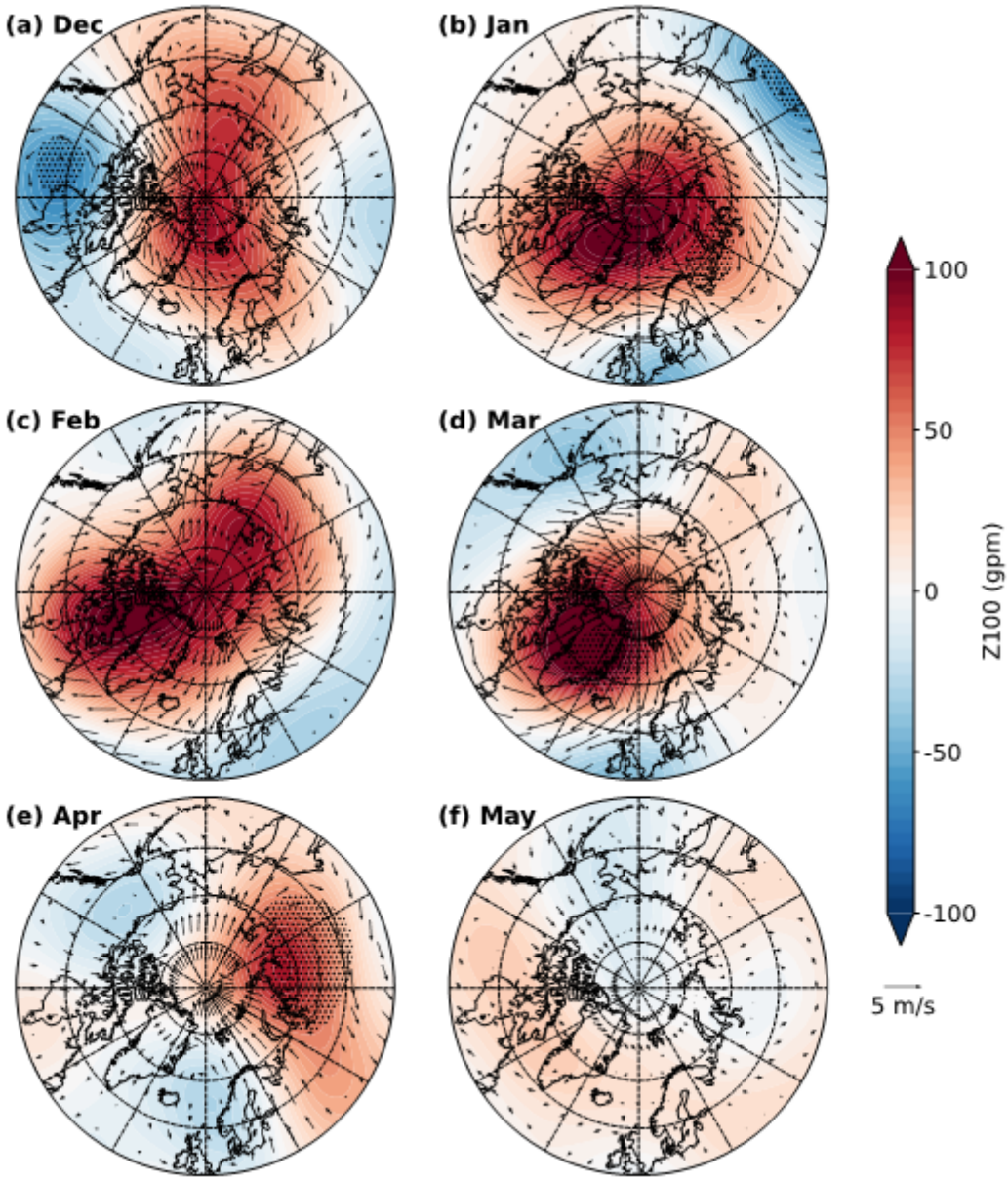

Figure 4

Z100 composite maps for the following December to May, relative to the detrended autumn SIE in BKS below 0.8 standard deviation (low SON SIE). The dots highlight significant anomalies at a confidence level of 95%

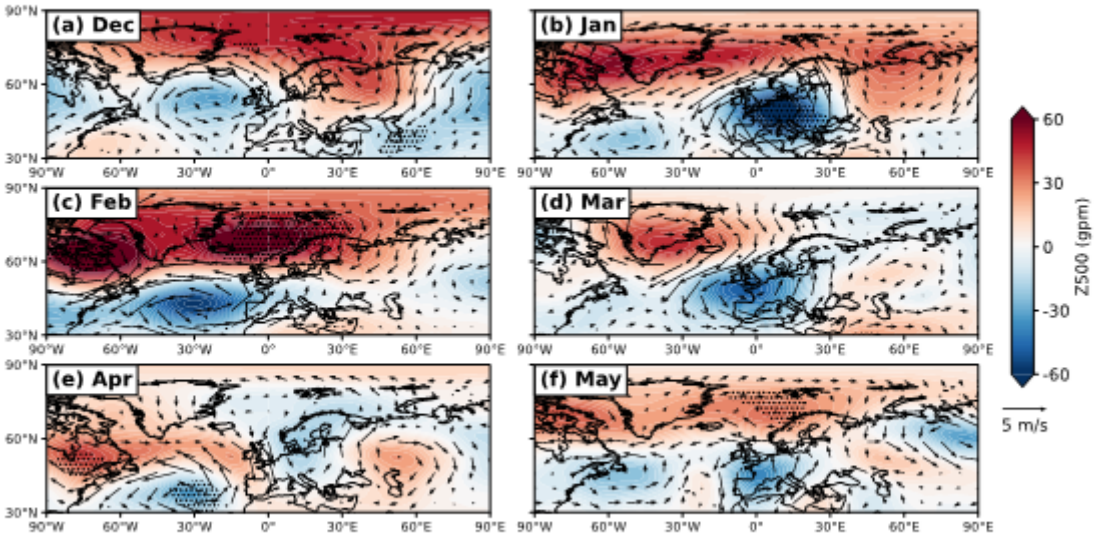

Figure 5

Z500 composite maps for the following December to May, relative to the detrended autumn SIE in BKS below 0.8 standard deviation (low SON SIE). The dots highlight significant anomalies at a confidence level of 95%

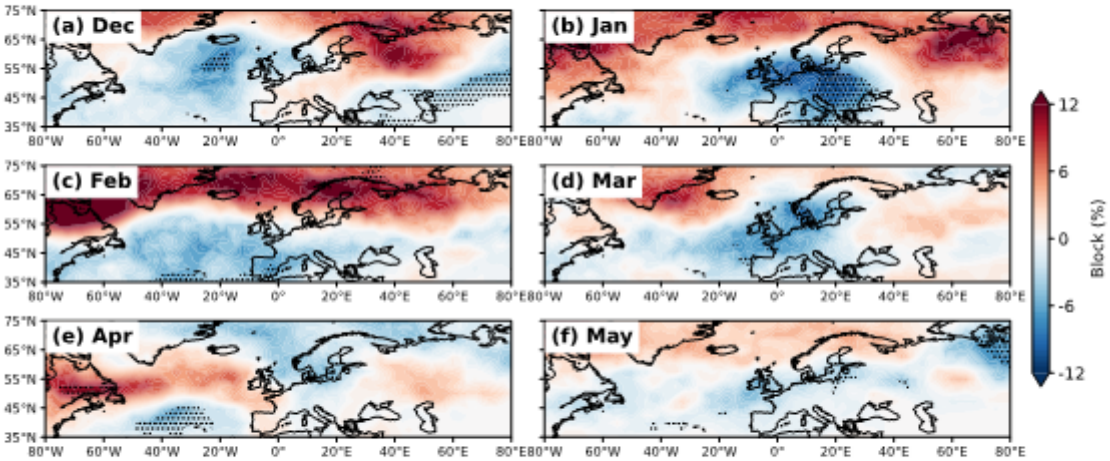

Figure 6

Blocking frequency composite maps for the following December to May, relative to the detrended autumn SIE in BKS below 0.8 standard deviation (low SON SIE). The dots highlight significant anomalies at a confidence level of 95%

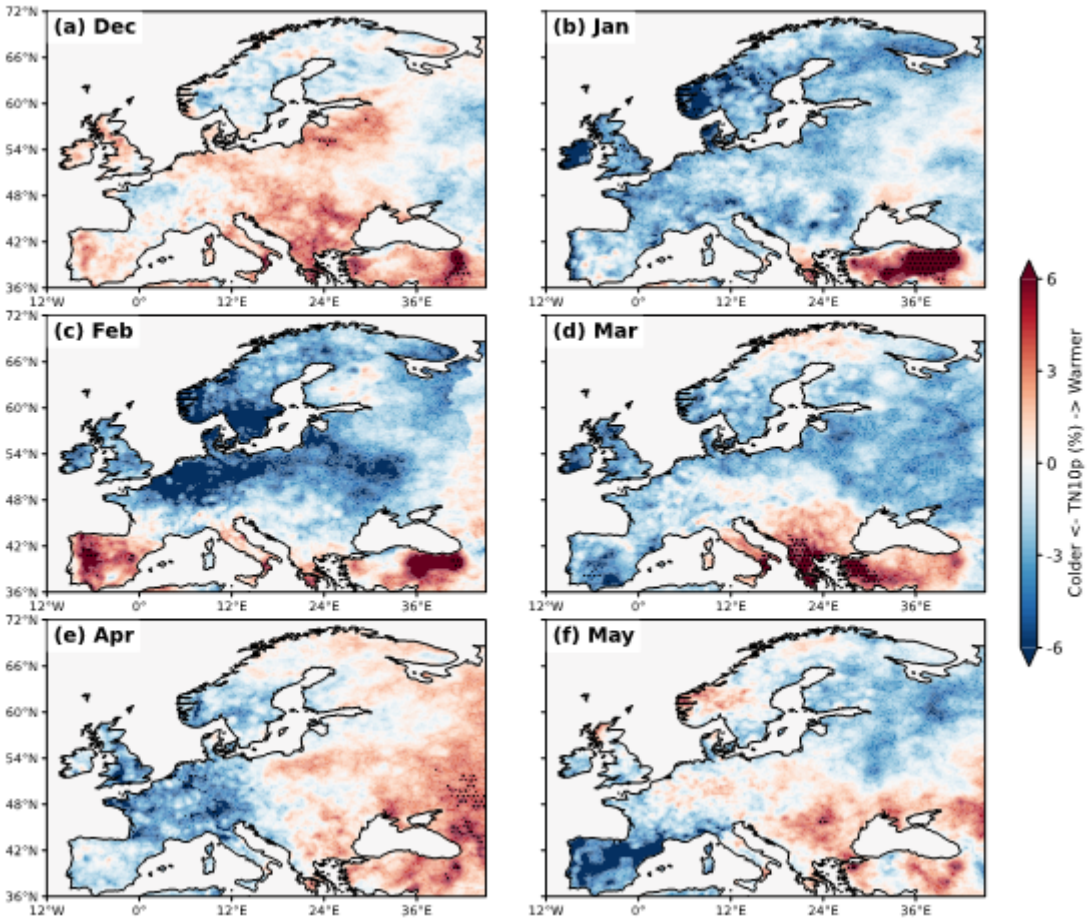

Figure 7

TN10p composite maps for the following December to May, relative to the detrended autumn SIE in BKS below 0.8 standard deviation (low SON SIE). Note that a negative sign is added for better understanding. The dots highlight significant anomalies at a confidence level of 95%